Biointerface Research in Applied Chemistry
Platinum Open Access Journal (ISSN: 2069-5837)

Article
Volume 12, Issue 6, 2022, 8515 - 8526
https://doi.org/10.33263/BRIAC126.85158526

Azo-dye Antibacterial with Nanotube-$[SiO_2(OH)_2]_9$ System for Drug Delivery Investigation

Majid Monajjemi [1], Fatma Kandemirli [1,*], Fatemeh Mollaamin [1]

[1] Department of Biomedical Engineering, Faculty of Engineering and Architecture, Kastamonu University, Kastamonu, Turkey
* Correspondence: fkandemirli@yahoo.com (F.K.);

Scopus Author ID 6602393314
Received: 28.10.2021; Revised: 27.11.2021; Accepted: 29.11.2021; Published: 12.12.2021

Abstract: Azo dye, $[SiO_2(OH)_2]_9$ molecular ring, and single-walled carbon nanotubes (4,4) SWCNT were considered like an axle, a wheel, and stoppers, respectively. The combination of the azo dye on the $[SiO_2(OH)_2]_9$ molecular ring with (4,4) SWCNTs may be thought of as a non-covalent system in UV light-isomer- machine. A new molecular motor system that runs like a hinge motion is demonstrated like light-powered molecular hinges. A new molecular motor system that acts as a hinge motion has been demonstrated and introduced as light-moving molecular hinges. By emitting various ultraviolet, visible lights, the $[SiO_2\,(OH)_2]_9$ molecular ring in the system can be reversed with the various dumb-bell size on one side attached halogens and fixing it on the other side of the (4,4) SWCNTs surface, a variety of systems in a wide variety of ultraviolet sensors can be designated to a better model of molecular machines and can be used for drug delivery of some antibiotics that are difficult to administer by straight injection. Molecular machines containing a wide variety of ultraviolet sensors have been designed with the combination of azo derivatives formed by replacing different halogens with hydrogen in the azo dye on the $[SiO_2(OH)_2]_9$ molecular ring to the (4,4) SWCNTs surface.

Keywords: nanotube carbons; molecular motor; rotaxane; switchable sensor.

1. Introduction

After the concept of Richard Feynman, synthetic or artificial molecular machines and engines in chemistry and nanotechnology have been one of the ultimate goals [1].

An important molecular class of machines, molecular motors use a variety of energy sources to design one-way mechanical movement. Working principles of those engines, whether biological or artificial, are different from the macroscopic engines of humans. Molecular motors in nano-scale sizes operate especially in a solution media having a viscosity. Under extremely damped conditions, a low Reynolds number means they cannot rely on inertia to maintain motion [2].

There are studies on the design and synthesis of “molecular actuators” that can change their shape in response to external effects resulting in mechanical work.

Up to the present, most of the researches has focused on ’‘rotaxanes' and ’‘catennes' [3-9] and biomolecular structures, which are more elaborate than classical cis-trans isomerism, and on bistable systems like machines based on the transition of right-handed to left-handed DNA. These systems, in which motion is changed by chemical, electrochemical or photochemical forces, are defined as molecular machines.

They summarized the recent developments regarding catenanes and rotaxanes, which display more complex molecular machine functions. They stated that these next-generation synthetic molecular machines are constantly moving out of equilibrium and can be considered true prototype molecular motors. The principles they derive are far from any classes of structural molecular machines and indeed far from equilibrium. They reported that it could be applied to other chemical processes of that process [10-12].

There are several kinds of molecular motors in nature that perform extremely sensitive and complex microscopic studies found in biological systems like ATPase, myosin, dimeric kinesin, and dynein. It may be classified as thermal, electrical, chemical [13,14], and light-powered molecular motors according to different driving forces.

Many molecular motors, like catenins and rotaxanes, have been synthesized and characterized [15-18]. Rotaxanes are usually surrounded by a macromolecular ring (route) and assembled from a molecule (ax-like) disconnected by a flat sheet or a bulky group to avoid disassembling [16].

Our aim in this work is to simulate azo dye as an azo-benzene-derived molecule inside $[SiO_2\ (OH)_2]_9$ molecular ring, while the (4,4) SWCNTs are used as a stopper as an axle and a wheel, respectively (Figure. 1). For the design of photo-isomer-controlled machines, a complex system can be used in which an azo dye molecule is placed on the $[SiO_2(OH)_2]_9$ molecular ring.

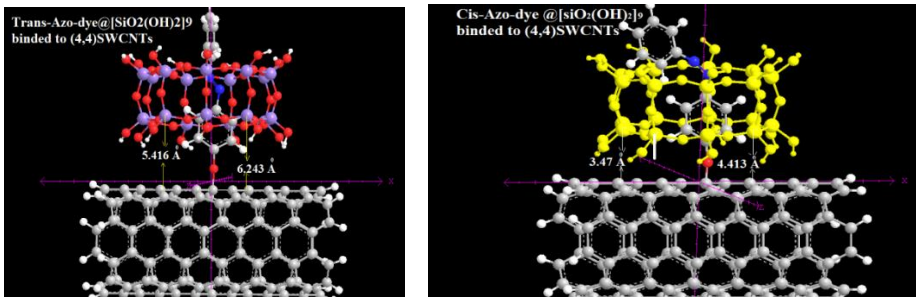

Figure 1. Optimized of the molecular motor including cis & trans isomers of azo dye over the surface of (4,4) SWCNTs & $[SiO_2(OH)_2]_9$.

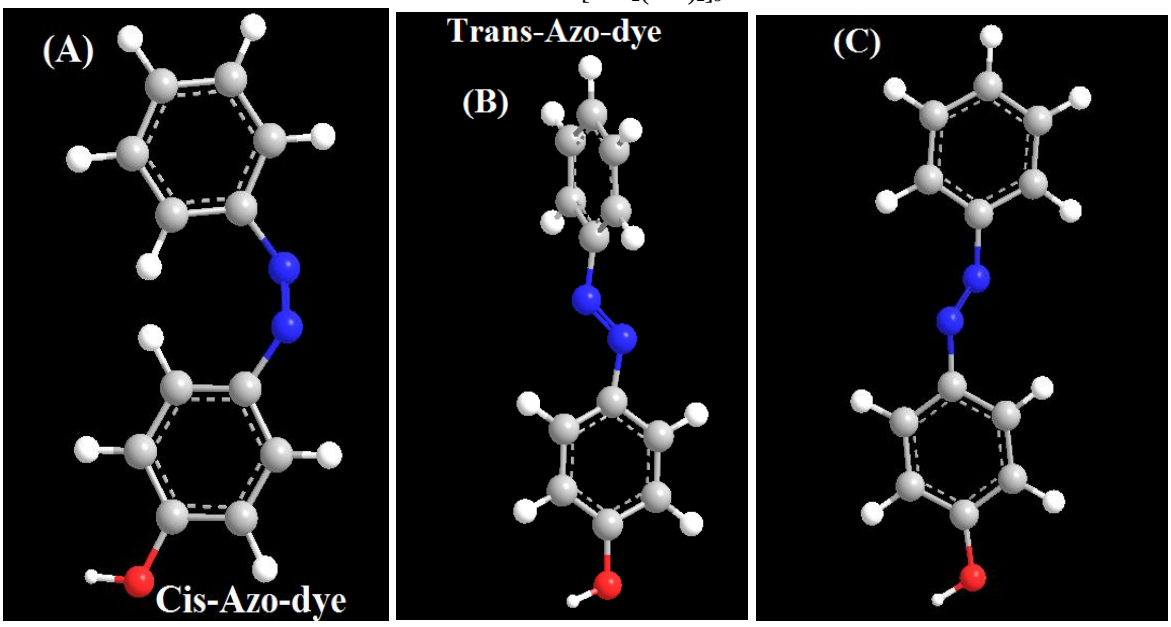

Figure 2. Various dihedral conformational of azo dye in several torsions degree of CNNC dihedrals (A=135º, B=90º, C=45º).

Therefore, the rational combination of (4,4) SWCNTs and the azo dye may offer a new avenue of research given that the presentation of azo dye on (4,4) SWCNTs has not been performed before.

This study reports a machine design based on (4,4) SWCNTs with azo dye embedded on a photo-exchangeable-on (4,4) SWCNTs. To achieve this aim, a considered machine was formed with two stopper-sides having (4,4) SWCNTs and dumb-bell-shaped components of -SO_2NH- part of azo dye (Figures 1 and 2).

The $[SiO_2(OH)_2]_9$ molecular ring with hydrophobic cavities acts as a host to form a special system with the azo dye molecule as the axis. Then, those were attached to the surface of (4,4) SWCNTs via oxygen atom (another part of azo dye molecule), and thus, (4,4) SWCNTs behave like the second stopper on the other side of the machine. The $[SiO_2(OH)_2]_9$ molecular ring in the system over the (4,4) SWCNTs surface can go back and forth along the azo dye molecule axes between the dumbell components driven by cis-trans isomerization of the N=N part of the azo dye molecule upon alternating irradiation [19] with UV-lights.

1.1. Cis-trans isomerization of azo-benzene.

Photoisomerization is the most interesting feature of azobenzene and azobenzene-derivatives. Azo dye molecules' cis and trans isomers can be reversibly interchanged by applying UV light of wavelength > 400 nm. This photochemical property of azobenzene-based compounds is the reason for their photosensitive behavior, making them suitable for use in various applications, such as developing various sensors. When UV light of the appropriate wavelength is given on the molecular system, the thermodynamically more stable trans form isomerizes to the cis form [20,21].

We aimed to demonstrate a new molecular motor system known as light-guided molecular hinges [22] that works like a hinge movement.

A hinge-like molecule[23] contains two sides connected to its edge sides via an axis, and a molecular hinge provides closing and opening of the system. For azo dye in (4,4)SWCNTs systems, we demonstrated that our machine has strong absorption of UV-visible lights and causes strong absorption of UV-visible lights at 306.1nm, corresponding to a π-π^* transition. This absorption was disappeared after irradiation shows that the simulated system is affected by the trans form and cis form.

One of the most important main properties of azobenzene is that it can change from the cis form to the trans form when it absorbs UV rays. Due to this property, it is widely used as light-sensitive materials [24-26], liquid crystals [27,28], electronic devices [29], or NLO chromophores [30].

Azobenzene-based compounds are widely used in liquid crystal (LC) materials, photosensitive materials, electronic devices, or NLO chromophores due to the ability of azo compounds to reversibly change their shape upon illumination (photoisomerization) [24-26]

Azo derivatives have versatile biological activities such as antimicrobial, anthelmintic, anti-inflammatory, antiviral, and anticancer [31-33]. Phenazopyridine, a urinary tract analgesic, and sulfasalazine-containing drugs for inflammatory bowel disease are typical examples of azo dye compounds. After the discovery of the first sulfonamide drug, it was opened a new era in medicine [34]

A new step in medicine was opened with the discovery of the first sulfonamide drug. Phenazopyridine, a urinary tract analgesic, and drugs containing sulfasalazine used for inflammatory bowel disease are drugs containing azo dye compounds.

2. Materials and Methods

2.1. Computational details.

The (4,4) SWCNTs, $[SiO_2(OH)_2]_9$ molecular ring, and azo dye that makes up the parts of the machine have been individually optimized using ab initio DFT calculations.

The whole system, that is, the whole sheet of the $[SiO_2(OH)_2]_9$ molecular ring and the azo dye axis (4,4) SWCNTs, was performed with the use of QM/MM.

The difference between the force fields was found by comparing the intensities and energies obtained with the OPLS and AMBER force fields. Besides, Hyper-Chem professional version 7.01 program with the PM3MM, PM6 (pseudo=lanl2) keywords have been used.

The result situation of the cis-trans form of the azo dye molecule was performed using SCF to calculate the optimal initial structures for these conformational structures and the different energies (Figures 2 and 3). DFT investigated van der Waals densities to model the variation correlation estimation. GAMESS-US package10 was used to optimize (4,4) SWCNTs layers.

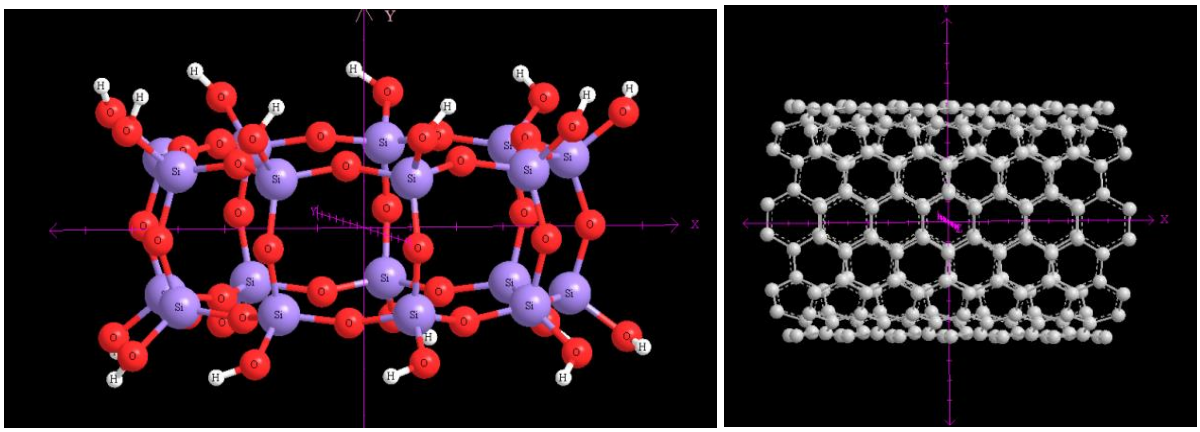

Figure 3. Optimized $[SiO_2(OH)_2]_9$ molecular ring and optimized (4,4) SWCNTs.

A Cis-trans conformation was calculated by using m062x, m06-L, and m06. This is because the m06-HF levels are a convenient consistency in uncoupled calculations between two isomers. Calculations in the non-covalent interactions between the $[SiO_2(OH)_2]_9$ molecular ring and the azo dye molecule, the level is high (H) for azo dye, medium (M), for $[SiO_2(OH)_2]_9$ molecules, and low (L) for (4,4) SWCNT' were performed using ring ONIOM methods. The high (H) layer, Medium layer, and low layer are performed using DFT, pm6, and MM, respectively.

Merz-Kollman-Singh [35], chelp [36], and chelp-G [37] were used to calculate both the charge transfer and electrostatic potentials. The interaction energies between the various structures of the azo dye contained in the $[SiO_2(OH)_2]_9$ molecular ring were calculated according to the following equation for each case:

$$\Delta E_i(eV) = \left\{E_{sys} - (E_{h-BN} + E_{[SiO_2(OH)_2]_9 \text{ molecular ring}} + E_{\text{azo dye}}\right\} + E_{BSSE} \quad (1)$$

where the "ΔE_i" states the energy for the various structures of azo dye in the $[SiO_2(OH)_2]_9$ molecular ring. A multifunctional wave-function analyzer was used to compute several properties, including electron spin densities, orbital wave-function values, the exchange-correlation densities, both electron localization function (ELF) and localized orbital locator (LOL), electron densities, the average local ionization energies, and total electrostatic potential (ESP) of both cis-trans isomers for oxygen bridge [38-40]. This molecular machine has been

evaluated for non-bonded interactions ELF, LOL, and structures of stator and rotor motors studied in the previous works [41-48].

3. Results and Discussion

In this work, the azo dye axis was modeled including SO_2NH_2, as a stopper at one side and the O-(4,4) SWCNTs's bridge at the other side (Figure 1).

As seen from Table 1, the wavelength of the machine system is 306.1nm which is closely related to the peaks obtained in the visible region performed by Hong Yan and co-workers [49] (Figure 1). In this work, a stereoisomer is shown in which the secondary side of the $[SiO_2(OH)_2]_9$ molecular ring; here, the bond formed by two oxygens with carbon acts as a stopper. It has also been shown that in the molecular ring $[SiO_2(OH)_2]_9$ as in Rotaxan, the movement of the azo dye between cis-trans units varies (Figure 2 and Table 1).

Theoretically, two peaks at 306.1nm and 245.03nm were observed in the UVA and UVB regions of the two systems of azo dye and F-azo dye machines. These peaks agree with the experimental results [49] obtained from the trans-cis isomers. As it can be seen in Figure 1, the $[SiO_2(OH)_2]_9$ molecular ring is located quite far from the surface of primarily (4.4) SWCNTs when the azo dye is in the trans-state, and then the $[SiO_2(OH)_2]_9$ molecular ring moves towards the (4 ,4) SWCNTs sheet position.

Contrary to the previous position, the trans-cis conversion of the azo dye system appears at the upper wavelength, so the forward and rear-wheel movement of the $[SiO_2(OH)_2]_9$ molecular ring through the azo dye depends on the two states of the rotaxane-functionalized (4,4) SWCNTs, and this is essentially useful for any light sensor.

When the groups such as Br, F, and Cl are attached to the second phenyl ring instead of NH_2, it is interestingly observed that the wavelength of the molecular machinery shifts down to the UVB regions for the F group UVB for the Cl and Br groups.

In this study, we aim to determine the partial electron density, Hamiltonian kinetic energy K(r), potential energy density U(r), LOL, ELF, and the average of the various atoms when Br, F, and Cl groups replace the NH_2 group attached to the phenyl group in the azo dye system.

The electron density can be written as:

$$\rho(r) = \eta_i \left|\varphi_i(r)\right|^2 = \sum_i \eta_i \left|\sum_l C_{l,i}\,\chi_i(r)\right|^2 \qquad (2)$$

where the"η_i" is orbital's occupation number. Although the amount of these parameters for the oxygen atom bound to (4,4)SWCNTs in the Br-azo dye and Cl-azo dye system is much different than the azo dye machine, F-azo dye parameters were found to be similar to the parameters obtained for azo dye. One of the reasons is that the electronegativity of oxygen is higher when chlorine and bromine groups are attached to the azo dye than when fluorine is attached to the azo dye.

Table 1. The $\Delta E_{Trans\text{-}Cis}$ for various machines as the photoswitchable sensors.

Axle systems (cis) to trans	$\Delta E_{Trans\ to\ Cis}$ the energy of motor including (axle, wheel, and stopper) (Hartree)	$\Delta E_{Trans\ to\ Cis}$ For Switch (Kcal/mole) & Cm^{-1} respectively	The barrier energy For Switching (eV)	Wavelength(nm), Frequency (THZ)	Region of Photo switchable sensor	Situation
F- azo dye)	0.036334	22.8, 7974.4	5.12	242.16, 1238.5	C (UVB)	Medium-wave, mostly absorbed by the ozone layer
Cl - azo dye	0.038406	24.1, 8429.1	5.65	219.5, 1366.2	C (UVC)	Short Wave, germicidal, completely absorbed by the ozone layer and atmosphere

Axle systems (cis) to trans	$\Delta E_{Trans\ to\ Cis}$ the energy of motor including (axle, wheel, and stopper) (Hartree)	$\Delta E_{Trans\ to\ Cis}$ For Switch (Kcal/mole) & Cm^{-1} respectively	The barrier energy For Switching (eV)	Wavelength(nm), Frequency (THZ)	Region of Photo switchable sensor	Situation
Br - azo dye	0.040637	25.5, 8918.8	5.73	216.3. 1385.5	C (UVC)	Short Wave, germicidal, completely absorbed by the ozone layer and atmosphere
azo dye	0.035537	22.3, 7799.5	4.32	287.0, 1044.6	A (UVA)	Long-wave, blacklight, not absorbed by the ozone layer

Bader [50] found that large electron localization can have large Fermi-hole and Becke and Edgecombe [51] values based on Bader's theory. The proposed electron localization function (ELF) for the relationship between Fermi hole and spin pair probability can be written by the following equation

$$ELF(r) = \frac{1}{1+[D(r)/D_{0(r)}]^2} \qquad (3)$$

where

$$D(r) = \frac{1}{2}\sum_i \eta_i \ |\nabla\varphi_i|^{\ 2} - \frac{1}{8}[\frac{|\ |\nabla\rho_\alpha|^{\ 2}}{\rho_\alpha\,(r)} + \frac{|\ |\nabla\rho_\beta|^{\ 2}}{\beta(r)}] \qquad (4)$$

and

$$D_{0(r)} = \frac{3}{10}(6\pi^2)^{\frac{2}{3}}[\rho_\alpha\,(r)^{\frac{5}{3}} + \rho_\beta\,(r)^{\frac{5}{3}}] \qquad (5)$$

It gives an ELF relative localization that varies only in the range [0, 1]. At values up to 1, ELF describes that the electrons are completely localized and at large values an unshared electron pair, a covalent bond, or the inner shells of atoms. As it can be seen in Table 2, (4,4) SWCNTs (O*) ELF for oxygen is greater than LOL in Cl-azo dye and Br-azo dye systems (for both cis and trans), but for F-azo dye and azo dye, this amount is smaller.

As seen from Table 2, the ELF in all systems is less than 0.5 means that the oxygen electron for the bridge of -(4,4) SWCNTs is not localized and provides flexibility to move it back and forth between the azo dye axis like rotaxane.

For trans-azo dye and trans-F-azo dye, this flexibility is greater than for trans-Br-azo dye and trans-Cl-azo dye machines due to the spatial barrier of Cl and Br compared to F (Table 3).

Savin et al. [52] examined ELF in terms of kinetic energies; Here, D(r) gives the extreme kinetic energy densities caused by the Pauli repulsion, and D_0(r) gives the Thomas-Fermi kinetic energies.

Table 2. The physical properties of oxygen-(4,4) SWCNTs(O*) bond in various systems of azo dye derivation in the same machine.

O*-SWCNTs in various Axle systems (azo dye)	Lumo/Homo Gap (kcal/mol) A orbitals β orbitals	ELF & LOL	Local information entropy	U(r) & K(r)	$\sum LIE$ & ESP
-cis (O)	2.99 3.10	0.140, 0.380	0.734	0.245, -0.132	0.769, -0.631
trans (O)	1.12 4.21	0.112, 0.344	0.715	-0.135, -0.431	0.815, -0.649
	2.89 3.21	0.151, 0.138	0.712	-0.213, -0.132	0.739, -0.723
	1.35 4.15	0.316, 0.167	0.865	-0.165, -0.136	0.740, -0.658
	2.17 1.35	0.243, 0.138	0.733	-0.142, -0.138	0.706, -0.633
	2.38 1.29	0.322, 0.155	0.835	-0.154, -0.120	0.811, -0.644
	2.54 1.45	0.147, 0.422	0.722	0.242, -0.141	0.651, -0.603
	3.16 1.67	0.113, 0.313	0.821	-0.151, -0.79	0.723, -0.608

As seen in Tables 1 and 2, the difference in Hamiltonian kinetic energies between trans isomers is greater in F-azo dye than in cis Cl-azo dye and Br-azo dye machines; meanwhile, cis-azo dye and cis-F-Azo dye potential energy density is positive for other systems and

negative for other systems. Since cis-Br-azo dye and cis-Cl-azo dye molecular motors have larger wavelengths (UVB & UVA), it is difficult to move back and forth (Table 2). Whereas cis-azo dye and cis-F-azo dye molecular motors are easier to move because they have higher energy and shorter wavelengths (UVC).

Table 3. Displacement distances from trans to cis of CD between two dumb-bell components.

Displacements	Trans distance	Displacement of Right side (angstrom)	Displacement of Left side (angstrom)
azo dye -machine	3.99	1.61	1.71
F- azo dye -machine	3.85	1.55	1.74
Cl- azo dye -machine	3.61	1.40	1.45
Br- azo dye -machine	3.49	1.35	1.49

The formula given for LOL expression is defined by Schmider and Becke [38].

$$LOL(r) = \frac{\tau(r)}{1+\tau(r)}, where\ (r) = \frac{D_0(r)}{\frac{1}{2}\sum_i \eta_i\ |\nabla\varphi_i|^{\ 2}} \qquad (6)$$

Although LOL and ELF contain similar expressions, LOL (Figure 4) gives more precise and clearer images than ELF.

According to Eq.6, LOL can be represented in the kinetic energy path, unlike ELF; Since the gradient of the orbital wave function is large (small) in the boundary regions of the localized orbit, the small (large) LOL magnitude is usually seen in the boundary regions of the localized orbit. In fact, LOL in Table 2 is greater than ELF in cis and trans form for both azo dye and F-azo dye systems and smaller for Cl-azo dye, and Br-azo dye systems support the previous discussion (Figure 5).

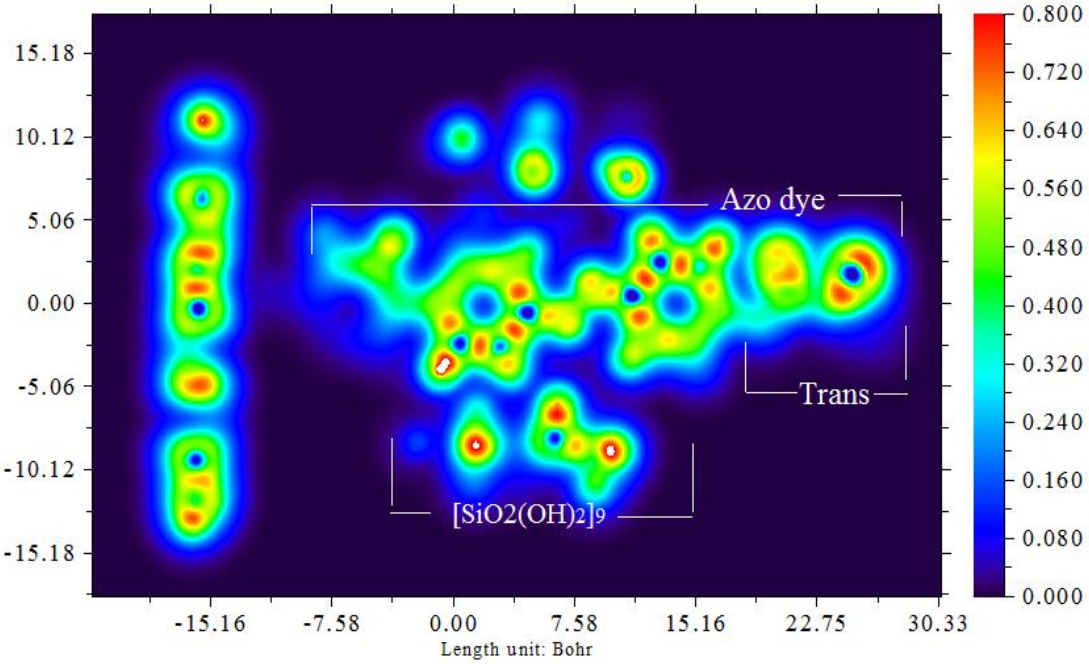

Figure 4. Color-field Map of ELF for $[SiO_2(OH)_2]_9$ molecular ring and for trans, isomers of an azo dye, which indicates the geometries.

According to Eq.6, LOL can be represented in the kinetic energy path, unlike ELF; Since the gradient of the orbital wave function is large (small) in the boundary regions of the localized orbit, the small (large) LOL magnitude is usually seen in the boundary regions of the localized orbit. In fact, LOL in Table 2 is greater than ELF in cis and trans form for both azo dye and F-azo dye systems and smaller for Cl-azo dye, and Br-azo dye systems support the previous discussion (Figure 5).

The data of molecular electrostatic potential and average local ionization energy values are given in Table 2. ESP has been widely used to predict molecular recognitions and intermolecular interaction of O-(4,4) SWCNTs bonds. Estimation of molecular recognitions and intermolecular interactions of O-(4,4) SWCNTs bonds can be made with total electrostatic potentials ESP. That is, the ESP gives information about the electrostatic interaction between the oxygen point charges (Figure 6).

As seen from Table 2, all data are approximately equal, and negative means that the current position is dominated by nuclear charges (not electronic charges). That means that it is independent of halogen radii and depends only on the surface properties of (4,4) SWCNT. For functional groups-azo dye (4,4) the distances between the plate of SWCNTs and the αCD are unequal on the right and left sides of the machines along the N-azo dye axis (Figure 7 & Table 3), which indicates that (4,4) SWCNTs deviate from the surface caused the $[SiO_2(OH)_2]_9$ molecular ring in the machine over the (4,4) The surface of SWCNTs can easily go back and forth along the azo dye axis. As seen in Table 3, the closeness of these distances to the right (or left) change indicates that this movement is monotonous in that direction (Figure 7).

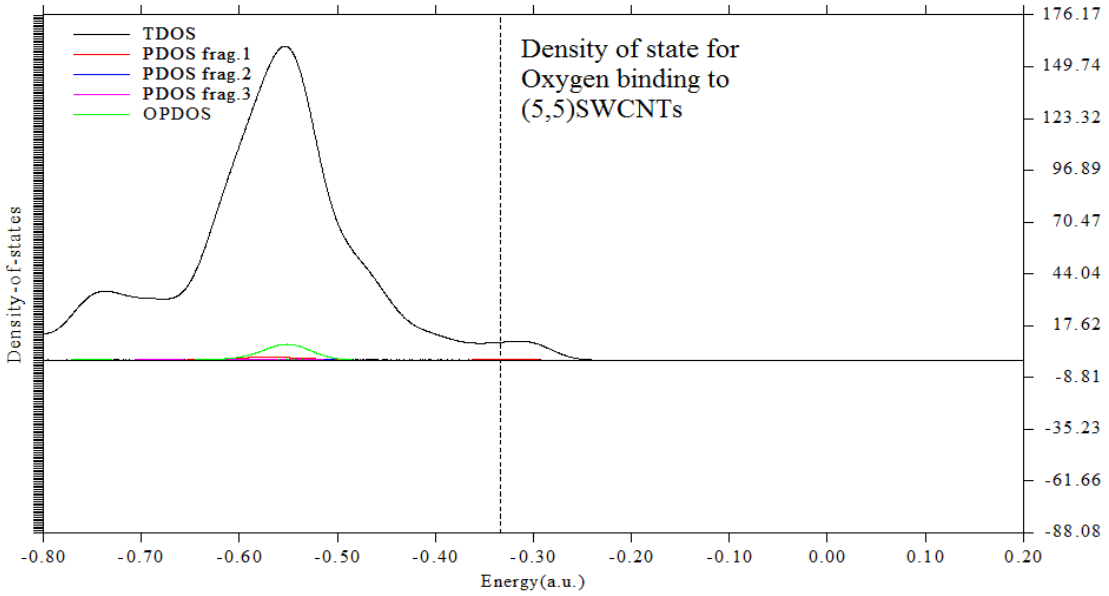

Figure 5. Electron densities for O-(4,4) SWCNTs.

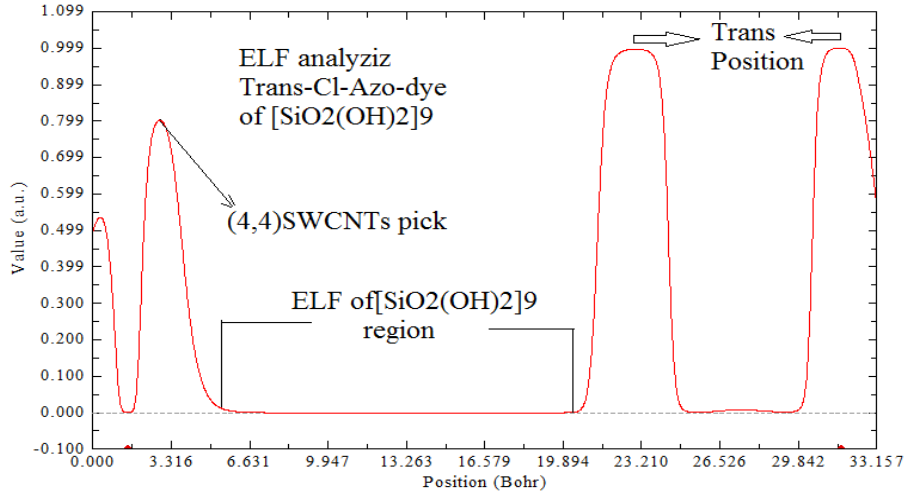

Figure 6. ELF Calculation for Cl-azo-dye-molecular motor.

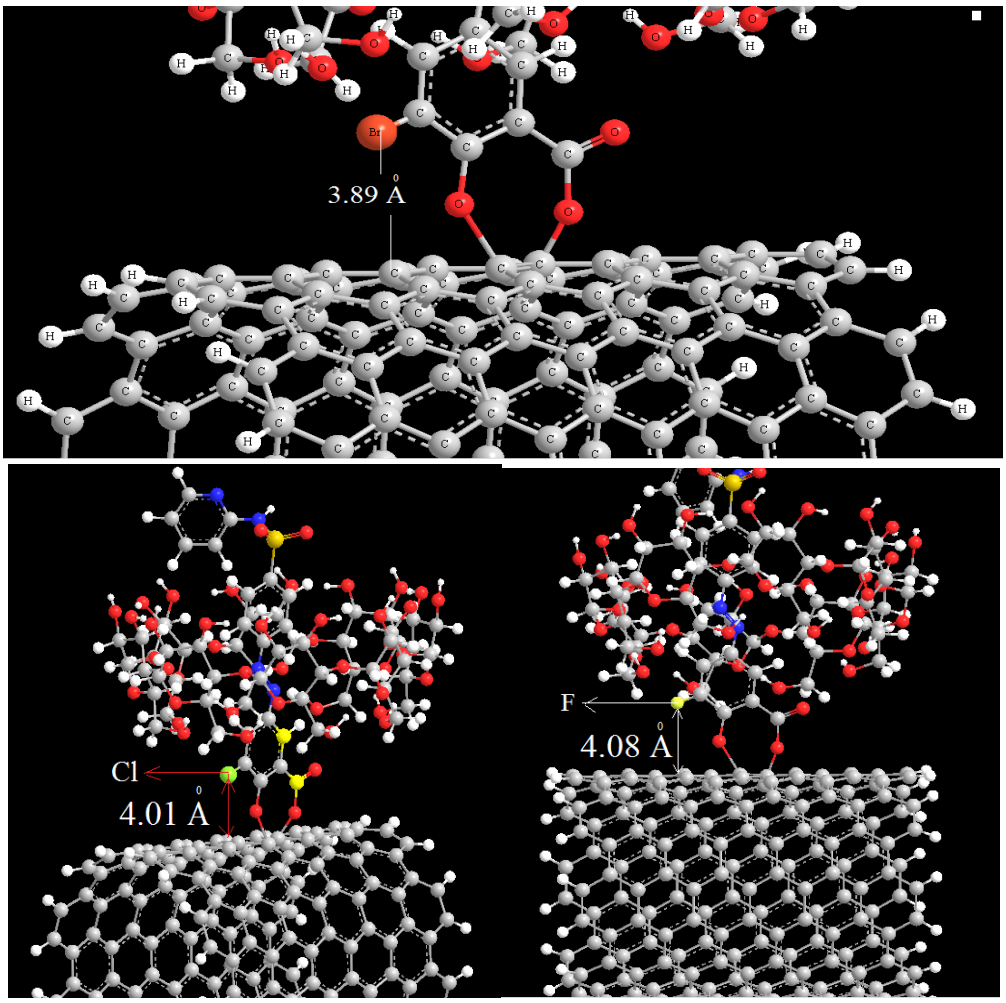

Figure 7. The distances between (4,4) SWCNTs and $[SiO_2(OH)_2]_9$ molecular ring for optimized azo dye (cis & trans), Cl- azo dye (trans), F- azo dye (trans), and Br- azo dye (trans) machines along the axis.

Carbon NMR values of the azo dye were calculated by the S-NICS method (Figure 8), and it was shown that azo compounds could be used as a drug carrier system.

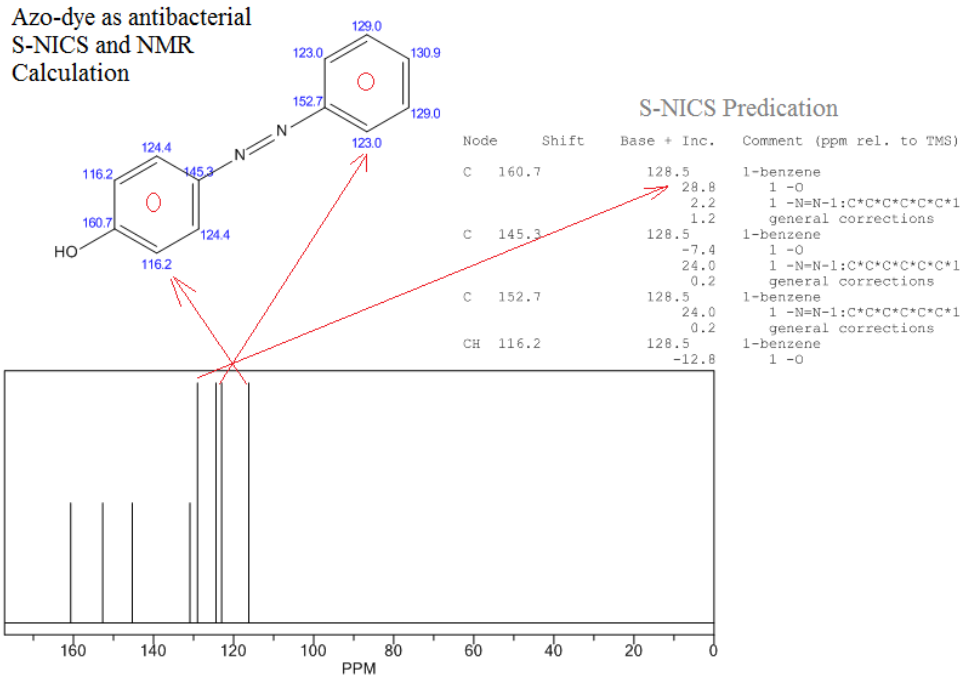

Figure 8. The carbon NMR shielding of Azo dye.

4. Conclusions

It has been shown that azo compounds can be used as a drug carrier system from the carbon NMR values of the Azo dye calculated by the S-NICS method. ESP predicted the molecular recognition and intermolecular interaction of O-(4.4) SWCNTs bonds and gave information about the electrostatic interaction between oxygen point charges. Systems for UV sensors related to the design of molecular machines are simulated by replacing the functional groups on one side with halogens and fixing the other side of the dumbbell ring. Such machines could be suitable for drug delivery in nanotechnology subjects.

Funding

This research received no external funding.

Acknowledgments

This research has no acknowledgment.

Conflicts of Interest

The authors declare no conflict of interest.

References

1. Feynman, R.P. There's Plenty of Room at the Bottom. *Caltech Eng. Sci*. **1960**, *23*.
2. Purcell, E.M. Life at Low Reynolds-Number. *Am. J. Phys*. **1977**, *45*, https://doi.org/10.1119/1.10903.
3. Sauvage, J.P. Transition Metal-Containing Rotaxanes and Catenanes in Motion: Toward Molecular Machines and Motors Acc. *Chem. Res*. **1998**, *31*, 611–619, https://doi.org/10.1021/ar960263r.
4. Balzani, V.; Gomez-Lopez, M.; Stoddart, J.F. Molecular Machines. *Acc. Chem. Res*. **1998**, *31*, 405–414, https://doi.org/10.1021/ar970340y.
5. Schröder, H.V.; Zhang, Y.; Link, A.J. Dynamic covalent self-assembly of mechanically interlocked molecules solely made from peptides. *Nature Chemistry* **2021**, *13*, 850-857, https://doi.org/10.1038/s41557-021-00770-7.
6. Evans, N.H. Macrocycles, Catenanes and Rotaxanes. In: *Reactivity in Confined Spaces*. **2021**; pp. 1-28, https://doi.org/10.1039/9781788019705-00001.
7. Pilon, S.; Jørgensen, S.I.; van Maarseveen, J.H. [2]Catenane Synthesis via Covalent Templating. *Chemistry—Chem. Eur. J*. **2021**, *27*, 2310–2314, https://doi.org/10.1002/chem.202004925.
8. Chan, S.-M.; Tang, F.-K.; Lam, C.-Y.; Kwan, C.-S.; Hau, S.C.K.; Leung, K.C.-F. π-Stacking Stopper-Macrocycle Stabilized Dynamically Interlocked [2]Rotaxanes. *Molecules* **2021**, *26*, https://doi.org/10.3390/molecules26154704.
9. Caprice, K.; Pál, D.; Besnard, C.; Galmés, B.; Frontera, A.; Cougnon, F.B.L. Diastereoselective Amplification of a Mechanically Chiral [2]Catenane. *J Am Chem Soc*. **2021**, *143*, 11957-11962, https://doi.org/10.1021/jacs.1c06557.
10. Kay, E.R.; Leigh, D.A. Beyond switches: Rotaxane- and catenane-based synthetic molecular motors. *Pure Appl Chem*. **2008**, *80*, 17-29, https://doi.org/10.1351/pac200880010017.
11. Blanc, F.E.; Cecchini, M. An Asymmetric Mechanism in a Symmetric Molecular Machine [opens in a new tab]open_in_new *J. Phys. Chem. Lett*. **2021**, *12*, https://doi.org/10.1021/acs.jpclett.1c00404.
12. Cera, G.; Arduini, A.; Secchi, A.; Alberto Credi, A.; Serena Silvi, S. Heteroditopic Calix[6]arene Based Intervowen and Interlocked Molecular Devices. *Chem. Rec*. **2021**, *21*, 1161–1181, https://doi.org/10.1002/tcr.202100012.
13. Kelly, T.R.; Cai, X.L.; Damkaci, F.; Panicker S.B.; Tu, B.; Bushell, S.M.; Cornella, I.; Piggott, M.J.; Salives, R.; Cavero, M.; Zhao, Y.; Jasmin, S. Progress toward a Rationally Designed, Chemically Powered Rotary Molecular Motor. *J Am Chem Soc*. **2007**, *129*, 376–386, https://doi.org/10.1021/ja066044a.
14. Yadav, S.; Kunwar, A. Temperature-Dependent Activity of Motor Proteins: Energetics and Their Implications for Collective Behavior. *Front Cell Dev Bio.* **2021**, *9*, https://doi.org/10.3389/fcell.2021.610899.
15. Yan, H.; Teh, C.; Sreejith, S.; Zhu, L.; Kwok, A.; Fang, W.; Ma, X.; Nguyen, K.T.; Korzh, V.; Zhao, Y. Functional Mesoporous Silica Nanoparticles for Photothermal-Controlled Drug Delivery In Vivo. *Angew. Chem. Int. Ed*. **2012**, *51*, 8373–8377, https://doi.org/10.1002/anie.201203993.

16. Balzani, V.; Credi, A.; Venturi, M. General Concept. In: *Molecular Devices and Machines – A Journey into the Nano World.* Wiley-VCH, Weinheim, Published Online: Volume 23, **2004**; https://doi.org/10.1002/3527601600.ch1.
17. Sauvage, J.P.; Dietrich-Buchecker, C. *Molecular Catenanes, Rotaxanes and Knots*. Wiley VCH, Weinheim, Germany, WILEY-VCH Verlag WILEY-VCH Verlag GmbH, D-69469 Weinheim, **1999**.
18. Iino, R.; Kinbara, K.; Bryant. Z. Introduction: Molecular Motors. *Chem Rev*. **2020,** *8*, 1-4, https://doi.org/10.1021/acs.chemrev.9b00819.
19. Ashton, P.R.; Ballardini, R.; Balzani, V.; Credi, A.; Dress, K.R.; Ishow, E.; Kleverlaan, C.J.; Kocian, O.; Preece, J.A.; Spencer, N.; Stoddart, J.F.; Venturi, M.; Wenger, S. A Photochemically Driven Molecular-Level Abacus. *Chem. Eur. J*. **2000**, *6*, https://doi.org/10.1002/1521-3765(20001002)6:19<3558::AID-CHEM3558>3.0.CO;2-M.
20. Bandara, H.M.D.; Friss, T.R.; Enriquez, M.M.; Isley, W.; Incarvito, C.; Frank, H.A.; Gascon, J.; Burdette, S.C. Proof for the Concerted Inversion Mechanism in the trans→cis Isomerization of Azobenzene Using Hydrogen Bonding To Induce Isomer Locking *J. Org. Chem*. **2010** *75*, 4817–4827, https://doi.org/10.1021/jo100866m.
21. Pirone, D.; Bandeira, N.A.G.; Tylkowski, B.; Boswell, E.; Labeque, R.; Garcia Valls, R.; Giamberini, M. Contrasting Photo-Switching Rates in Azobenzene Derivatives: How the Nature of the Substituent Plays a Role. *Polymers* **2020**, *12*, https://doi.org/10.3390/polym12051019.
22. Hamilton, A.D.; Van Engen, D. Induced fit in synthetic receptors: nucleotide base recognition by a molecular hinge. *J. Am. Chem. Soc*. **1987**, *109*, 5035-5036, https://doi.org/10.1021/ja00250a052.
23. Shinkai, S.; He, G. X.; T. Matsuda, A. D. Hamilton, H.S. Rosenzweig, Specific inhibition of flavin catalyses by a "molecular hinge" *Tetrahedron Lett.* **1989**, *30*, 5895–5898, https://doi.org/10.1016/S0040-4039(01)93499-9.
24. Parenti, F.; Morvillo, P.; Bobeico, E.; Diana, R.; Lanzi, M.; Fontanesi, C.; Tassinari, F.; Schenetti, L.; Mucci, A.; Eur. (Alkylsulfanyl)bithiophene-alt-Fluorene: π-Conjugated Polymers for Organic Solar Cells. *J. Org. Chem*. **2011**, *2011*, 5659–5667, https://doi.org/10.1002/ejoc.201100738.
25. Hrozhyk, U.A.; Serak, S.V.; Tabiryan, N.V.; Hoke, L.; Steeves, D.M.; Kimball, B.; Kedziora, G. Systematic Study of Absorption Spectra of Donor–Acceptor Azobenzene Mesogenic Structures. *Molecular Crystals and Liquid Crystals* **2008**, *489*, 257/[583]-272/[598], https://doi.org/10.1080/15421400802218959.
26. Kempfer-Robertson, E.M.; Thompson, L.M. Effect of Oriented External Electric Fields on the Photo and Thermal Isomerization of Azobenzene. *J Phys Chem A*. **2020**, *124*, 3520-3529, https://doi.org/10.1021/acs.jpca.0c00492.
27. Caruso, U.; Diana, R.; Panunzi, B.; Roviello, A.; Tingoli, M.; Tuzi, A. Facile synthesis of new Pd(II) and Cu(II) based metallomesogens from ligands containing thiophene rings. Inorg. Chem. Commun. **2009**, *12*, 1135–1138, https://doi.org/10.1016/j.inoche.2009.09.006.
28. Arakawa, Y.; Komatsu, K.; Ishida, Y.; Tsuji H. Thioether-linked azobenzene-based liquid crystal dimers exhibiting the twist-bend nematic phase over a wide temperature range. *Liquid Crystals* **2021**, *48*, 641-652, https://doi.org/10.1080/02678292.2020.1800848.
29. Angiolini, L.; Benelli, T.; Giorgini, L.; Golemme, A.; Mazzocchetti, L.; Termine, R. Effect of a chiral substituent on the photochromic and photoconductive properties of a methacrylic polymer bearing side chain azocarbazole moieties. *Dyes Pigm*. **2014**, *102*, 53–62, https://doi.org/10.1016/j.dyepig.2013.10.024.
30. Caruso, U.; Diana, R.; Fort, A.; Panunzi, B.; Roviello, A. Synthesis of Polymers Containing Second Order NLO-Active Thiophene and Thiazole Based Chromophores. *Macromol. Symp., Wiley Online Library: Naples, Italy* **2006**, *234*, 87–9, https://doi.org/10.1002/masy.200650212.
31. Mitra A. K.; Mawson, A.R. Neglected Tropical Diseases: Epidemiology and Global Burden. *Trop Med Infect Dis.* **2017**, *2*, https://doi.org/10.3390/tropicalmed2030036.
32. O'Brien, S. *All-Party Parliamentary Group on Malaria and Neglected Tropical Diseases (APPMG)*. WHO, Geneve, Switzerland, 2008; pp. 1–15.
33. Sari, S.; Koçak, E.; Kart, D.; Özdemir, Z.; Acar, M.F.; Sayoğlu, B.; Karakurt, A.; Dalkara, S. Azole derivatives with naphthalene showing potent antifungal effects against planktonic and biofilm forms of Candida spp.: an in vitro and in silico study. *International Microbiology* **2021**, *24*, 93-102, https://doi.org/10.1007/s10123-020-00144-y.
34. Hager T. *The Demon Under the Microscope: From Battlefield Hospitals to Nazi Labs, One Doctor's Heroic Search for the World's First Miracle Drug*. Harmony Books **2006**.
35. Besler, B.H.; Merz, K.M.; Kollman, P.A. Atomic charges derived from semiempirical methods *J. Comp. Chem*. **1990**, *11*, 431-439, http://dx.doi.org/10.1002/jcc.540110404.
36. Chirlian, L.E.; Francl, M.M. Atomic charges derived from electrostatic potentials: A detailed study. *Journal of Computational Chemistry* **1987**, *8*, 894-905, https://doi.org/10.1002/jcc.540080616.
37. Breneman C.M.; Wiberg, K.B. Determining atom-centered monopoles from molecular electrostatic potentials – the need for high sampling density in formamide conformational-analysis. *J. Comp. Chem* **1990 11,** 361-373. https://doi.org/10.1002/jcc.540110311.
38. Lu, T.; Chen, F. Multiwfn: A multifunctional wave-function analyzer. *J. Comp. Chem*. **2012**, *33*, 580-592, https://doi.org/10.1002/jcc.22885.

39. Lu, T.; Chen, F. Calculation of Molecular Orbital Composition. *Acta Chimica Sinica -Chinese Edition* **2011**, *69*, 2393-2406.
40. Lu, T.; Chen, F.J. Quantitative analysis of molecular surface based on improved Marching Tetrahedra algorithm. *Mol. Graph. Model* **2012**, *38*, 314-323, https://doi.org/10.1016/j.jmgm.2012.07.004.
41. Monajjemi, M.; Lee, V.S.; Khaleghian, M.; Honarparvar, B.; Mollaamin, F. Theoretical Description of Electromagnetic Nonbonded Interactions of Radical, Cationic, and Anionic NH2BHNBHNH2 Inside of the B18N18 Nanoring. *The Journal of Physical Chemistry C* **2010**, *114*, 15315-15330, https://doi.org/10.1021/jp104274z.
42. Monajjemi, M. Non bonded interaction between BnNn (stator) and BN(-,0,+)B (rotor) systems: A quantum rotation in IR region. *Chemical Physics* **2013**, *425*, 29-45, https://doi.org/10.1016/j.chemphys.2013.07.014.
43. Monajjemi, M. Cell membrane causes the lipid bilayers to behave as variable capacitors: A resonance with self-induction of helical proteins. *Biophysical Chemistry* **2015**, *207*, 114-127, https://doi.org/10.1016/j.bpc.2015.10.003.
44. Monajjemi, M. Metal-doped graphene layers composed with boron nitride–graphene as an insulator: a nano-capacitor. *J Mol Model* **2014**, *20*, 2507, https://doi.org/10.1007/s00894-014-2507-y
45. Monajjemi, M.; Boggs, J.E. A New Generation of BnNn Rings as a Supplement to Boron Nitride Tubes and Cages. *The Journal of Physical Chemistry A* **2013**, *117*, 1670-1684, https://doi.org/10.1021/jp312073q.
46. Monajjemi, M. Liquid-phase exfoliation (LPE) of graphite towards graphene: An ab initio study. *Journal of Molecular Liquids* **2017**, *230*, 461-472, https://doi.org/10.1016/j.molliq.2017.01.044.
47. Monajjemi, M. Non-covalent attraction of B2N(−,0) and repulsion of B2N(+) in the BnNnring: a quantum rotatory due to an external field. *Theoretical Chemistry Accounts* **2015**, *134*, https://doi.org/10.1007/s00214-015-1668-9.
48. Arulaabaranam, K.; Muthu, S.; Mani, G.; Ben Geoffrey, A.S. Speculative assessment, molecular composition, PDOS, topology exploration (ELF, LOL, RDG), ligand-protein interactions, on 5-bromo-3-nitropyridine-2-carbonitrile. *Heliyon* **2021**, *7*, https://doi.org/10.1016/j.heliyon.2021.e07061.
49. Yan, H.; Zhu, L.; Li, X.; Kwok, A.; Pan, X.; Zhao, Y. A Photoswitchable [2]Rotaxane Array on Graphene Oxide. *Asian Journal of Organic Chemistry* **2012**, *1*, 314-318, https://doi.org/10.1002/ajoc.201200102.
50. Bader, R.F.W. *Atoms in Molecule: A quantum Theory* (Oxford Univ. press, Oxford), **1990.**
51. Becke, A.D.; Edgecombe, K.E, A simple measure of electron localization in atomic and molecular systems. *J. Chem. Phys.***1990**, *92*, https://doi.org/10.1063/1.458517.
52. Savin, A.; Jepsen, O.; Flad, J.; Andersen, O.K.; Preuss, H.; von Schnering , H.G. Electron Localization in Solid-state Structures of the Elements: the Diamond Structure. *Angew. Chem. Int. Ed.Engl.* **1992**, *31*, https://doi.org/10.1002/anie.199201871.